

Breaking the Tuning Barrier: Zero-Hyperparameters Yield Multi-Corner Analysis Via Learned Priors

Wei W. Xing
School of Mathematical and Physical
Science, University of Sheffield
Sheffield, UK
w.xing@sheffield.ac.uk

Kaiqi Huang
SZU-UoS Joint Centre for Innovation
and Entrepreneurship, College of
Mechatronics and Control Engineering,
Shenzhen University
Shenzhen, China

Jiazhan Liu
SZU-UoS Joint Centre for Innovation
and Entrepreneurship, College of
Mechatronics and Control Engineering,
Shenzhen University
Shenzhen, China

Hong Qiu
SZU-UoS Joint Centre for Innovation
and Entrepreneurship, College of
Mechatronics and Control Engineering,
Shenzhen University
Shenzhen, China

Shan Shen*
Nanjing University of Science and
Technology
Nanjing, China
shanshen@njjust.edu.cn

ABSTRACT

Yield Multi-Corner Analysis validates circuits across 25+ Process-Voltage-Temperature corners, resulting in a combinatorial simulation cost of $O(K \times N)$ where K denotes corners and N exceeds 10^4 samples per corner. Existing methods face a fundamental trade-off: simple models achieve automation but fail on nonlinear circuits, while advanced AI models capture complex behaviors but require hours of hyperparameter tuning per design iteration, forming the Tuning Barrier. We break this barrier by replacing engineered priors (i.e., model specifications) with learned priors from a foundation model pre-trained on millions of regression tasks. This model performs in-context learning, instantly adapting to each circuit without tuning or retraining. Its attention mechanism automatically transfers knowledge across corners by identifying shared circuit physics between operating conditions. Combined with an automated feature selector (1152D to 48D), our method matches state-of-the-art accuracy (mean MREs as low as 0.11%) with zero tuning, reducing total validation cost by over $10\times$.

1 INTRODUCTION

As integrated circuit technology advances, process variations such as intra-die mismatches, doping fluctuations, and threshold voltage shifts become critical design factors. For modern designs with highly replicated structures like SRAM cell arrays, yield analysis is essential. The ultimate challenge is Yield Multi-Corner Analysis (YMCA), where circuits must be validated across K Process-Voltage-Temperature (PVT) corners, often exceeding 25 configurations. This creates a combinatorial cost barrier: naive Monte Carlo simulation requires $O(K \times N)$ evaluations, where $N > 10^3$ samples per corner are needed for acceptable accuracy. For a 32-transistor SRAM across 25 corners, this translates to over 25,000 SPICE simulations requiring weeks of computation, making iterative design impractical.

The field’s pursuit of acceleration has followed two main paths, both reaching fundamental barriers. Importance Sampling (IS) methods like MNIS [1] achieved remarkable $100\times$ speedups through automated norm-minimization, becoming an industry standard. However, simple Gaussian priors create a model capacity barrier: single-point assumptions cannot capture complex, nonlinear failure regions of

Table 1: Hyperparameter sensitivity of relative error and # sim. on 8×2 SRAM with 10 configurations ($\pm 20\%$ variation).

		OPT [5]	FUSIS [6]	ACS [10]	HSCS [11]
MRE (%)	Mean	45.25	79.36	69.18	74.94
	Std. Dev.	28.96	102.43	37.75	44.60
	Best (Min)	19.36	12.35	11.92	11.11
	Worst (Max)	111.24	346.32	100.00	137.78
# Sim.	Mean	461k	26k	147k	195k
	Std. Dev.	56k	5k	65k	99k
	Best (Min)	343k	21k	42k	103k
	Worst (Max)	500k	34k	245k	437k
# HyperParam.		10	7	6	3

modern circuits [12]. Subsequent clustering approaches [10, 11] remained limited by their underlying strong model assumptions.

The second path pursued expressive surrogate-based acceleration [3]. Methods based on Gaussian Processes [14], deep kernels [13], and normalizing flows [5] successfully broke the model capacity barrier by learning complex, nonlinear failure boundaries. However, this power comes at a steep cost: careful hyperparameter tuning, including kernel selection and network architecture search. The SOTA performance, to some extent, is achieved by careful tuning for particular benchmark problems and is unable to generalize. Thus, these methods are rarely implemented in industrial environments.

Table 1 illustrates the severity of this Tuning Barrier. We evaluate state-of-the-art methods on the 8×2 SRAM benchmark with 10 hyperparameter configurations sampled within $\pm 20\%$ of recommended values. Results reveal extreme sensitivity: OPT [5] exhibits errors ranging from 19.36% to 111.24%, while HSCS [11] ranges from 11.11% to 137.78%. Even the simulation budget varies wildly—ACS [10] consumes between 42k and 245k samples depending on hyperparameter choices. This instability renders these methods unreliable for industrial deployment, where engineers cannot afford hours of expert tuning per design iteration only to face unpredictable performance. This barrier is compounded by multi-corner requirements: while methods like BI-BD [2] and BI-BC [8] exploit cross-corner correlation, they model only binary Pass/Fail outcomes, discarding continuous performance information that is critical for accurate yield estimation.

We resolve this impasse by replacing engineered priors with learned priors from meta-learning. Traditional methods encode priors through hand-crafted choices: GP kernels specify smoothness assumptions,

*Corresponding author.

while IS methods use Gaussian assumptions that sacrifice accuracy. Our framework employs TabPFN [4], a foundation model pre-trained on millions of regression tasks to learn optimal priors. When presented with circuit simulation data, TabPFN performs in-context Bayesian inference through a single forward pass, requiring zero hyperparameter optimization. The learned prior, encoded in pre-trained weights, adapts automatically through attention that identifies and exploits correlations across corners. This cross-corner knowledge transfer is ideal for YMCA: when predicting yield at a sparsely sampled corner, the model borrows strength from well-sampled correlated corners, dramatically improving efficiency.

Our framework integrates this zero-hyperparameter engine into a complete YMCA pipeline. An automated feature selection pipeline discovers sparse, physically interpretable parameter subsets, compressing 1152-dimensional (1152D) circuits to approximately 48 dimensions through single-pass training on initial samples. A global surrogate $\hat{P}(x, c)$ jointly models all corners, with uncertainty-driven active learning focusing simulations on decision boundaries where yield predictions matter most. Our contributions are:

- We identify the Tuning Barrier as the fundamental trade-off between model expressiveness and automation that has blocked industrial adoption of modern AI methods for yield analysis.
- We introduce a learned prior framework using foundation models to achieve expressive modeling with zero per-circuit tuning through in-context learning.
- We demonstrate automatic cross-corner knowledge transfer, with ablation studies showing over 70% error reduction on challenging corners through the learned prior.
- We develop a complete pipeline integrating automated feature selection (1152D to 48D) with zero-hyperparameter inference, achieving state-of-the-art accuracy (mean MREs as low as 0.11%) and robustness across volatile yield corners, while reducing total validation cost by over 10 \times .

2 THE BARRIERS OF YIELD ANALYSIS

2.1 Yield Multi-Corner Estimation

Consider a circuit characterized by a D -dimensional process variation vector $\mathbf{x} = [x_1, \dots, x_D]^T \in \mathcal{X}$. After standardization, components follow independent Gaussian distributions. The circuit must be validated across K PVT corners $C = \{c_1, \dots, c_K\}$, where each corner $c_k \in \mathbb{R}^p$ specifies voltage and temperature conditions. Performance at process point \mathbf{x} under corner c_k is determined by SPICE simulation $y_k = f(\mathbf{x}, c_k)$. The circuit passes if $f(\mathbf{x}, c_k) > \text{Spec}_{c_k}$. Yield at corner k is

$$Y_k = \int_{\mathcal{X}} \mathbb{I}[f(\mathbf{x}, c_k) > \text{Spec}_{c_k}] p(\mathbf{x}) d\mathbf{x}, \quad (1)$$

where $\mathbb{I}[\cdot]$ denotes the indicator function. Standard Monte Carlo estimation requires $N > 1000$ samples per corner for 3% relative error. For $K = 25$ corners, this demands over 25,000 SPICE runs with prohibitive $O(K \times N)$ cost.

2.2 Automation with Model Capacity Barrier

Importance Sampling methods replace the original distribution $p(\mathbf{x})$ with a proposal $q(\mathbf{x})$ concentrated on failure regions [9, 11]. MNIS [1] achieves massive speedups using a Gaussian proposal constructed from a single minimum-norm failure point. This engineered prior

enables full automation. More recent methods like EFIAL [12] improve upon MNIS by utilizing all failure samples rather than one, maintaining zero tuning cost.

However, these methods face a fundamental model capacity barrier. MNIS and EFIAL remain constrained by their Gaussian covariance assumptions, which cannot represent multi-modal or highly nonlinear failure boundaries. This creates systematic bias: accuracy plateaus at high error regardless of additional samples. As noted in [12], simple models overlook rich information from failure samples and cannot capture complex failure regions of modern circuits. This is the Model Capacity Barrier.

2.3 Expressiveness with Tuning Barrier

Surrogate-based methods overcome capacity limitations by constructing expressive approximations of the SPICE function or failure boundaries. Gaussian Processes [14], deep kernels [13], and normalizing flows [5] successfully broke the Model Capacity Barrier by capturing arbitrary nonlinearities through flexible model families. Recent work [6] demonstrates that SVM surrogates can construct quasi-optimal IS proposals, unifying surrogate and IS acceleration paths.

However, this expressiveness requires extensive hyperparameter optimization. A 100-dimensional circuit requires optimizing 100+ kernel lengthscales, architecture choices, and training hyperparameters through non-convex optimization, consuming hours per iteration. Critically, this tuning must be repeated for every design change. Table 1 quantifies this instability: state-of-the-art methods exhibit errors varying from 19% to 111% and simulation budgets from 42k to 245k samples under modest $\pm 20\%$ hyperparameter perturbations. This per-circuit tuning tax has blocked industrial adoption despite academic success. The field thus faces an impossible trade-off: methods achieve either automation (IS methods) or expressiveness (surrogate methods), but not both—this is the Tuning Barrier.

3 BREAKING THE TUNING BARRIER VIA LEARNED PRIORS

The Tuning Barrier arises from reliance on engineered priors: hand-crafted model specifications that are either too rigid (causing bias) or too flexible (requiring hyperparameter optimization). We replace this foundation with learned priors from meta-learning, eliminating per-circuit tuning while maintaining model expressiveness through a theoretically justified framework. Our approach operates in two stages: sparse feature selection identifies critical parameters, then a zero-hyperparameter inference engine performs efficient multi-corner yield estimation.

3.1 From Engineered to Learned Priors

The Bayesian posterior predictive distribution (PPD) provides the theoretical foundation for prediction under uncertainty. Given query point $\mathbf{z}^* = [\mathbf{x}^*, \mathbf{c}^*]^T$ combining process parameters and corner variables, and training observations $D_{\text{train}} = \{(\mathbf{z}_i, y_i)\}_{i=1}^n$, the PPD integrates over all hypotheses $\phi \in \Phi$ weighted by their posterior probability:

$$p(y^* | \mathbf{z}^*, D_{\text{train}}) = \int_{\Phi} p(y^* | \mathbf{z}^*, \phi) p(\phi | D_{\text{train}}) d\phi, \quad (2)$$

where the posterior $p(\phi | D_{\text{train}}) = p(D_{\text{train}} | \phi) p(\phi) / p(D_{\text{train}})$ follows Bayes' theorem. This integral is intractable for complex hypothesis

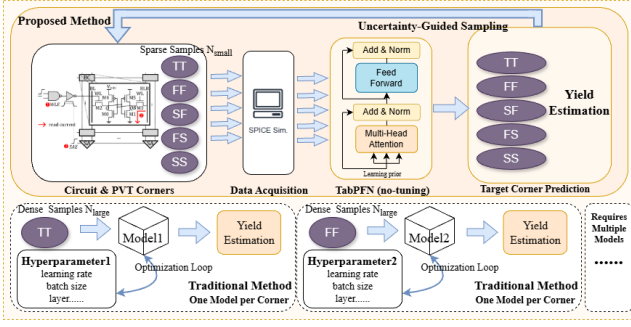


Figure 1: Automated YMCA framework. Sparse feature selection reduces the problem dimension within TabPFN’s capacity. The main loop alternates between in-context learning and uncertainty-driven active sampling until convergence.

spaces, necessitating approximation strategies that fundamentally determine the method’s expressiveness and automation trade-off.

Traditional Approximation: Point Estimates. Gaussian Processes approximate Eq. 2 by restricting the hypothesis space to a parametric family of kernels k_θ and finding a point estimate θ^* through marginal likelihood maximization:

$$\theta^* = \arg \max_{\theta} \log p(D_{\text{train}}|\theta) = \arg \max_{\theta} \log \mathcal{N}(y|0, K_\theta + \sigma^2 I), \quad (3)$$

where K_θ is the Gram matrix with entries $[K_\theta]_{ij} = k_\theta(z_i, z_j)$. For a D -dimensional circuit, this requires optimizing $O(D)$ lengthscales parameters plus kernel-specific hyperparameters through non-convex optimization. This constitutes the Tuning Barrier: each new circuit requires hours of optimization, and the point estimate θ^* ignores uncertainty in hyperparameter selection.

Meta-Learning Approximation: Amortized Inference. We adopt a fundamentally different approximation strategy that amortizes the cost of Bayesian inference across a distribution of functions. Rather than optimize θ for each circuit, we pre-train a neural network \mathcal{G}_Θ to directly approximate the posterior predictive distribution across a meta-distribution of functions $p_{\text{meta}}(f)$. This Prior-Fitted Network [4] is trained once via the meta-learning objective:

$$\Theta^* = \arg \min_{\Theta} \mathbb{E}_{f \sim p_{\text{meta}}(f)} \left[\mathbb{E}_{D_{\text{train}} \sim f} \left[\mathbb{E}_{(z^*, y^*) \sim f} [-\log p_\Theta(y^*|z^*, D_{\text{train}})] \right] \right], \quad (4)$$

where the expectations are taken over: (1) functions f sampled from the meta-prior $p_{\text{meta}}(f)$, (2) training sets D_{train} sampled from f , and (3) test points (z^*, y^*) sampled from f .

Theoretical Justification. The meta-learning objective in Eq. 4 can be understood as minimizing the KL divergence between the learned approximation $p_\Theta(y^*|z^*, D_{\text{train}})$ and the true PPD $p(y^*|z^*, D_{\text{train}})$ averaged over the meta-distribution:

$$\Theta^* = \arg \min_{\Theta} \mathbb{E}_{f, D_{\text{train}}, z^*} [\text{KL}(p(y^*|z^*, D_{\text{train}}) \| p_\Theta(y^*|z^*, D_{\text{train}}))]$$

This reveals that the meta-learning objective directly minimizes the expected prediction error under the true posterior predictive distribution, providing a principled foundation for the learned prior. At inference, the trained network performs in-context learning: it accepts new circuit data D_{circuit} as input and computes the approximate PPD through a single forward pass:

$$(\mu^*, (\sigma^*)^2) = \mathcal{G}_{\Theta^*}(z^*, D_{\text{circuit}}), \quad (5)$$

where μ^* and $(\sigma^*)^2$ parametrize the predictive distribution $p_{\Theta^*}(y^*|z^*, D_{\text{circuit}}) = \mathcal{N}(y^*|\mu^*, (\sigma^*)^2)$. Crucially, this requires no gradient descent, no hyperparameter optimization, and no retraining, eliminating the Tuning Barrier while maintaining Bayesian uncertainty quantification.

Architecture as Learned Kernel. We employ TabPFN [4], a Transformer architecture where the self-attention mechanism functions as a learned, nonlinear kernel. For a query point z^* and training set $D_{\text{circuit}} = \{(z_i, y_i)\}_{i=1}^n$, the attention mechanism computes:

$$\text{Attention}(z^*, D_{\text{circuit}}) = \text{softmax} \left(\frac{\mathbf{Q}(z^*)\mathbf{K}(D_{\text{circuit}})^T}{\sqrt{d_k}} \right) \mathbf{V}(D_{\text{circuit}}), \quad (6)$$

where \mathbf{Q} , \mathbf{K} , and \mathbf{V} are learned query, key, and value transformations with dimensionality d_k . This can be interpreted as a data-dependent kernel $k_{\text{learned}}(z^*, z_i; D_{\text{circuit}})$ that adapts to the structure of each new circuit through attention weights:

$$k_{\text{learned}}(z^*, z_i; D_{\text{circuit}}) \propto \exp \left(\frac{\mathbf{Q}(z^*)^T \mathbf{K}(z_i)}{\sqrt{d_k}} \right), \quad (7)$$

Unlike GP kernels that require per-circuit tuning, this kernel is fixed after pre-training yet automatically adapts to new circuits through the attention mechanism’s implicit conditioning on D_{circuit} .

3.2 Cross-Corner Knowledge Transfer

Rather than modeling each corner c_k independently (which would require K separate models and ignore cross-corner correlation), we formulate a unified global surrogate that learns shared circuit physics across all corners. This design choice enables automatic knowledge transfer between corners, dramatically improving sample efficiency.

Joint Input Representation. We concatenate sparse process parameters $\mathbf{x}_S \in \mathbb{R}^{|\mathcal{S}|}$ with corner encoding $c \in \mathbb{R}^p$ into a unified input vector:

$$\mathbf{z} = \begin{bmatrix} \mathbf{x}_S \\ c \end{bmatrix} \in \mathbb{R}^{|\mathcal{S}|+p}, \quad (8)$$

where the corner encoding c typically includes normalized voltage and temperature. This enables the global surrogate $\hat{f}(\mathbf{x}_S, c) : \mathbb{R}^{|\mathcal{S}|+p} \rightarrow \mathbb{R}$ to model performance across all corners simultaneously.

Cross-Corner Transfer. The attention mechanism in Eq. 6 automatically identifies and exploits cross-corner correlations. When predicting at a sparsely sampled corner c_j with training data $D_j = \{(z_i, y_i)\}$ where $\mathbf{z}_i = [\mathbf{x}_i^T, c_j^T]^T$, the attention weights

$$\alpha_{ij} = \exp \left(\frac{\mathbf{Q}(z^*)^T \mathbf{K}(z_i)}{\sqrt{d_k}} \right) / \sum_{i'} \exp \left(\frac{\mathbf{Q}(z^*)^T \mathbf{K}(z_{i'})}{\sqrt{d_k}} \right) \quad (9)$$

automatically upweight training samples from correlated corners $c_k \approx c_j$ with similar process parameters $\mathbf{x}_k \approx \mathbf{x}^*$. The attention mechanism distinguishes corners via the corner encoding c , preventing negative transfer between dissimilar corners (e.g., SS and FF).

Information Sharing Analysis. The global model enables information flow from well-sampled corners to sparsely sampled ones. Consider two corners c_1 (well-sampled, n_1 samples) and c_2 (sparse, $n_2 \ll n_1$ samples). For a prediction at (\mathbf{x}^*, c_2) , the sample size is

$$n_{\text{eff}}(\mathbf{x}^*, c_2) = \sum_{i=1}^{n_1+n_2} \alpha_i^2(\mathbf{x}^*, c_2; D_{\text{all}}) \geq n_2, \quad (10)$$

where $D_{\text{all}} = D_1 \cup D_2$ and α_i are normalized attention weights. When corners are correlated (similar circuit physics), samples from c_1 receive non-negligible attention weights, effectively increasing n_{eff}

beyond n_2 and improving prediction uncertainty. This cross-corner knowledge transfer is particularly valuable for YMCA, where the same circuit topology operates under different PVT conditions that share underlying physical mechanisms.

3.3 Uncertainty-Guided Active Learning

The Bayesian nature of TabPFN’s learned prior provides calibrated uncertainty estimates $\sigma(\mathbf{z})$ at no additional computational cost—a consequence of approximating the full posterior predictive distribution rather than a point estimate. We exploit this for principled active learning, focusing expensive SPICE simulations on regions where they provide maximum information gain for yield estimation.

Information-Theoretic Acquisition Function. For each corner c_k , we define an acquisition function balancing predictive uncertainty with proximity to the specification boundary Spec_k :

$$\alpha_k(\mathbf{x}) = \sigma(\mathbf{x}, c_k) \cdot \phi\left(\hat{f}(\mathbf{x}, c_k) - \text{Spec}_k / \sigma(\mathbf{x}, c_k)\right), \quad (11)$$

where $\phi(\cdot)$ is the standard Gaussian density and $\sigma(\mathbf{x}, c_k)$ is the predictive standard deviation from Eq. 5. This uncertainty-weighted boundary sampling has an elegant interpretation: the first term $\sigma(\mathbf{x}, c_k)$ captures epistemic uncertainty (reducible through more data), while the Gaussian density term $\phi(\cdot)$ concentrates sampling near the decision boundary where pass/fail classification is most uncertain. The product achieves maximum value at points that are both highly uncertain and near the specification, where additional samples provide maximum information about yield.

Multi-Corner Optimization. Since yield must be estimated simultaneously across all K corners, we optimize the joint acquisition:

$$\alpha(\mathbf{x}) = \max_{k \in \{1, \dots, K\}} \alpha_k(\mathbf{x}), \quad (12)$$

selecting the corner k^* and process parameters \mathbf{x}^* that maximize information gain across the entire PVT space. For batch parallel simulation (size B), we employ a greedy diversification strategy: after selecting \mathbf{x}_1^* , subsequent selections maximize $\alpha(\mathbf{x}) - \beta \sum_{b=1}^{j-1} \exp(-\|\mathbf{x} - \mathbf{x}_b^*\|^2 / 2\gamma^2)$ where the penalty term ($\beta, \gamma > 0$) encourages spatial diversity in the selected batch.

3.4 Scalability via Sparse Feature Selection

TabPFN’s learned prior is most effective for moderate-dimensional spaces ($D \leq 100$). Industrial circuits like 32×2 SRAMs with $D = 1152$ variation parameters exceed this range. However, circuit physics exhibits inherent sparsity: performance typically depends on a small subset of critical transistors rather than all 1152 parameters. We exploit this through an automated, zero-tuning feature selection pipeline that identifies critical parameters without introducing the hyperparameter optimization burden we seek to avoid.

Greedy Forward Selection Framework. Our approach employs a validation-driven greedy search guided by initial importance ranking. Given initial samples D_0 , we first train a Gradient Boosting Decision Tree (GBDT) model M_{gbdt} using default LightGBM configuration—no hyperparameter tuning required. GBDT models naturally produce feature importance scores $\{I_j\}_{j=1}^{D+p}$ as a byproduct of training, quantifying each feature’s aggregate contribution across all tree splits. We rank features by importance: $\mathcal{F}_{\text{ranked}} = (f_{(1)}, f_{(2)}, \dots, f_{(D+p)})$ where $I_{(1)} \geq I_{(2)} \geq \dots \geq I_{(D+p)}$.

With this ranking established, we split D_0 into training (D_{train} , 80%) and validation (D_{val} , 20%) subsets. For each candidate subset

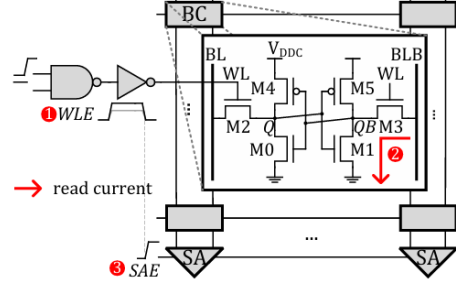


Figure 2: Read current path of 6T SRAM cell from OpenYield benchmark suite [7].

size $k \in \{1, 2, \dots, \lfloor (D+p)/B \rfloor\}$ where B is a fixed batch size, we construct \mathcal{S}_k containing the top $k \times B$ features from $\mathcal{F}_{\text{ranked}}$. A fresh GBDT model M_k is trained on D_{train} using only features in \mathcal{S}_k , and evaluated on D_{val} via R^2 score:

$$R^2(\mathcal{S}_k) = 1 - \frac{\sum_{(z,y) \in D_{\text{val}}} (y - M_k(z))^2}{\sum_{(z,y) \in D_{\text{val}}} (y - \bar{y}_{\text{val}})^2}, \quad (13)$$

where \bar{y}_{val} is the mean target value in D_{val} . The optimal subset is:

$$\mathcal{S}^* = \arg \max_k R^2(\mathcal{S}_k). \quad (14)$$

Zero-Tuning Guarantee. Critically, this entire pipeline requires no hyperparameter optimization. The GBDT models use fixed default configurations optimized for general small-sample scenarios, applied universally across all circuits and corners in our experiments without case-specific adjustments. The batch size $B = 10$ is a non-sensitive granularity parameter, not a tunable hyperparameter. Validation performance (Eq. 13) serves as the sole selection criterion (Eq. 14), eliminating manual hyperparameter choices. This one-time, sub-minute preprocessing typically compresses a 1152-dimensional SRAM array to approximately 48 dimensions ($|\mathcal{S}^*| \approx 48$), bringing them within TabPFN’s effective range while preserving physical interpretability.

This feature selection addresses a limitation of the current TabPFN implementation rather than a fundamental algorithmic constraint. The 500-feature limit stems from TabPFN’s training on datasets with up to 500 features—a practical choice given computational resources. If TabPFN were trained on higher-dimensional synthetic datasets (which our SCM/BNN prior can readily generate), it would naturally handle 1152-dimensional circuits directly. Our feature selection thus serves as an efficient preprocessing step for the current model, eliminating the need to retrain TabPFN while maintaining the zero-hyperparameter philosophy throughout the entire pipeline.

Algorithm 1 summarizes the complete procedure. Computational cost per iteration is dominated by SPICE simulation (minutes to hours); TabPFN inference via Eq. 5 and acquisition optimization complete in seconds due to the amortized inference paradigm. The algorithm converges when yield estimates stabilize: $\max_k |\hat{Y}_k^{(t)} - \hat{Y}_k^{(t-1)}| < \epsilon$ for convergence threshold ϵ .

4 EXPERIMENTAL VALIDATION

With the framework established, we now validate it on industrial SRAM benchmarks. We first outline the benchmark circuits and PVT conditions, then evaluate our method against Monte Carlo and state-of-the-art baselines under consistent metrics, with particular emphasis on total validation cost.

Benchmark Circuits. We use OpenYield’s industrial-quality SRAM macros in FreePDK45 (45 nm), which include critical peripherals—sense

Algorithm 1 Zero-Hyperparameter YMCA Framework

Require: Corners C , specifications $\{\text{Spec}_k\}$, budgets $N_{\text{total}}, N_{\text{init}}, B$
Ensure: Yield estimates $\{\hat{Y}_k\}_{k=1}^K$

- 1: **Initialize:** $D_0 \leftarrow \text{LHS-Sample-and-Simulate}(N_{\text{init}} \times K)$
 - 2: $\mathcal{S} \leftarrow \{1, \dots, D + p\}$ {Full feature set}
 - 3: **if** $D + p > 500$ **then**
 - 4: $\mathcal{S}^* \leftarrow \text{SelectFeatures}_{\text{Greedy}}(D_0, \text{Eq. 14})$
 - 5: $D_0 \leftarrow \text{Project}(D_0, \mathcal{S}^*)$
 - 6: $\mathcal{S} \leftarrow \mathcal{S}^*$ {Update to the optimal subset}
 - 7: **end if**
 - 8: $D_t \leftarrow D_0$
 - 9: **while** $|D_t| < N_{\text{total}}$ and not converged **do**
 - 10: **In-Context Learning:** $(\hat{f}_t, \sigma_t) \leftarrow \text{TabPFN}(D_t)$
 - 11: **Yield Estimation:** $\hat{Y}_k^{(t)} \leftarrow \text{EstimateYield}(\hat{f}_t, \mathcal{S}, M = 10^6)$
 - 12: **Active Learning:** $\{\mathbf{x}_b^*, k_b^*\}_{b=1}^B \leftarrow \text{Select}(\hat{f}_t, \sigma_t, \mathcal{S}, \text{Eq. 11})$
 - 13: **Simulate & Update:** $\{y_b^*\}_{b=1}^B \leftarrow \text{SPICE}(\{(\mathbf{x}_b^*, c_{k_b^*}^*)\}_{b=1}^B)$
 - 14: $D_{t+1} \leftarrow D_t \cup \{(\text{Project}(\mathbf{x}_b^*, \mathcal{S}), c_{k_b^*}^*, y_b^*)\}_{b=1}^B$
 - 15: **end while**
 - 16: **return** $\{\hat{Y}_k^{(t)}\}_{k=1}^K$
-

Table 2: PVT Combinations used in our experiments. The process corners in the context represent a PVT combination.

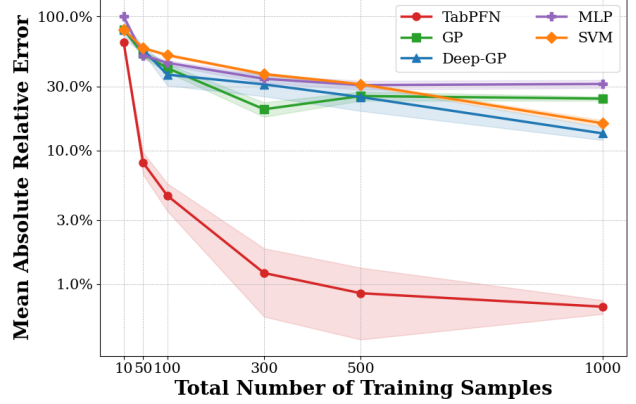
Process Corner	TT	FF	SF	FS	SS
Voltage (V)	1.0	1.1	1.0	1.0	0.9
Temperature (C)	25	0	25	25	125
#Simulations	10k	10k	10k	10k	10k

Table 3: SRAM configurations used in our experiments. The number of rows spans 4–32, while the number of columns remains 2 for faster simulations.

Testcase	1	2	3	4
#Row	4	8	16	32
#Column	2	2	2	2
Delay Spec (ns)	0.0626	0.0745	0.113	0.209
#Process Para.	144	288	576	1152

amplifiers (SA), column mux, wordline drivers, and decoders—and capture second-order effects (parasitics, leakage, and PVT variations) [7]. As illustrated in Figure 2, a read operation precharges both bitlines and then asserts the wordline to connect the storage node through the access transistor; a read failure occurs when variations prevent sufficient bitline differential within the delay specification or induce a read disturb. We evaluate five PVT corners (TT, SS, FF, FS, SF) across four array sizes: 4×2 , 8×2 , 16×2 , and 32×2 . These realistic testcases comprised of full peripheral circuits on the read path highlight the proposed model’s robustness across corner conditions and SRAM sizes. Tables 2 and 3 summarize the operating conditions and configurations.

Baseline Methods. For YMCA, we compare against Monte Carlo (MC) as the unbiased reference; BI-BD and BI-BC [2, 8], which exploit cross-corner correlation; and OPT [5], a complex-model-driven yield analysis with corner transfer capacity. For single-corner yield analysis, we include Importance Sampling (IS) baselines: the industry-standard MNIS [1], and more recent methods HSCS [11] and ACS [10].


Figure 3: Surrogate model comparison on 8×2 SRAM. TabPFN (red) exhibits superior data efficiency in the small-sample regime while requiring zero hyperparameter tuning.

Prior evaluations typically use idealized SRAM bitcells without peripherals or second-order effects; in contrast, our comparisons are run on realistic macro-level OpenYield testcases, ensuring results that reflect practical conditions.

Evaluation Metrics. To ensure consistent comparisons, we report accuracy and efficiency using relative error $\text{error} = |\hat{Y} - Y|/Y \times 100\%$ against the golden MC reference, Mean Relative Error (MRE) $\text{MRE} = \frac{1}{K} \sum_{k=1}^K |\text{error}_k|$ across corners, and speedup $S = N_{\text{MC}}/N_{\text{method}}$. Critically, we evaluate the total validation cost by combining simulation time. When convenient, we also use the failure rate $P_{\text{fail}} = 1 - Y$ as an equivalent yield metric.

4.1 TabPFN versus Traditional Surrogates

To assess our learned-prior engine’s competitiveness, we compare TabPFN against traditional surrogates, including Gaussian Process (GP), Deep-GP, MLP, and SVM, on the 8×2 SRAM benchmark. To ensure the comparison reflects fundamental model capacity rather than insufficient effort, all baseline methods were tuned using 5 random search to find the best results, whereas TabPFN was applied with fixed defaults and zero tuning.

Figure 3 shows TabPFN’s superior data efficiency in the small-sample regime (< 1000). Baselines do show early status due to their unstable performance. Around 100 samples, TabPFN achieves low error ($\sim 5\%$ MAE), while all tuned baselines lag significantly, with MAE ranging from $\sim 30\%$ (GP) to over $\sim 45\%$ (MLP). As the budget increases, all methods improve, but TabPFN maintains a clear margin while eliminating tuning overhead. This confirms that learned priors deliver strong modeling efficiency without per-circuit training, making them well-suited as the core of our framework.

4.2 Single-Corner Yield Analysis

We assess yield analysis in a challenging single-corner setting: the 8×2 SRAM at the FF corner. This checks whether the proposed method delivers the top performance in a challenging single-corner yield analysis problem.

Figure 4 illustrates the yield estimation convergence. IS methods (HSCS, ACS) exhibit pronounced cold-start phases: errors remain high while hundreds of simulations are spent exploring to locate failure regions. In contrast, our approach avoids this overhead. With

Table 4: Detailed yield predictions for all methods across PVT corners. Ground truth results Y (%) from 50,000-sample MC, predicted yield \hat{Y} (%), and MRE. The lowest MRE per corner is bolded.

Circuit	Method	TT			FF			SF			FS			SS		
		Y	\hat{Y}	MRE(%)												
4×2	BI-BD	100	100	0	95.0	95.4	0.42	90.9	91.2	0.33	100	100	0	0	0	0
	BI-BC	100	100	0	95.0	96.4	1.47	90.9	91.6	0.77	100	100	0	0	0	0
	OPT	100	100	0	95.0	95.9	0.94	90.9	92.2	1.43	100	100	0	0	0	0
	Proposed	100	100	0	95.0	95.4	0.42	90.9	90.8	0.11	100	100	0	0	0	0
8×2	BI-BD	87.1	87.4	0.34	99.0	99.2	0.20	11.3	11.2	0.89	100	100	0	0	0	0
	BI-BC	87.1	88.8	1.95	99.0	98.4	0.61	11.3	12.4	9.73	100	100	0	0	0	0
	OPT	87.1	88.5	1.61	99.0	99.4	0.40	11.3	29.9	100+	100	100	0	0	0	0
	Proposed	87.1	87.3	0.23	99.0	99.0	0.01	11.3	11.4	0.88	100	100	0	0	0	0
16×2	BI-BD	31.5	36.2	14.9	100	100	0	0.14	0	100+	97.8	98.6	0.82	96.1	94.9	1.25
	BI-BC	31.5	32.0	1.59	100	100	0	0.14	0.50	100+	97.8	98.3	0.51	96.1	96.8	0.73
	OPT	31.5	45.6	44.8	100	100	0	0.14	22.1	100+	97.8	97.9	3.07	96.1	96.9	3.85
	Proposed	31.5	31.7	0.63	100	100	0	0.14	0.20	42.8	97.8	97.5	0.31	96.1	96.6	0.52
32×2	BI-BD	97.6	97.9	0.31	100	100	0	34.9	48.0	37.5	100	100	0	85.0	86.9	2.24
	BI-BC	97.6	98.0	0.41	100	100	0	34.9	37.0	6.02	100	100	0	85.0	86.5	1.76
	OPT	97.6	97.4	3.07	100	100	0	34.9	54.1	55.0	100	100	0	85.0	87.6	3.05
	Proposed	97.6	97.7	0.10	100	100	0	34.9	36.0	3.15	100	100	0	85.0	86.9	2.24

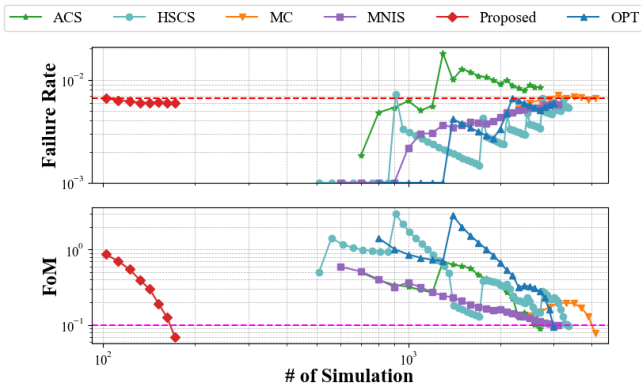


Figure 4: Convergence on single challenging corner (8×2 SRAM, FF corner) of SOTA yield analysis methods.

Table 5: Single-corner performance on 8×2 SRAM FF corner against 4,100-sample MC baseline.

Method	P_{fail}	MRE (%)	#Sim.	Speedup
MC	6.59×10^{-3}	—	4100	—
OPT	6.00×10^{-3}	8.88	3000	1.4x
MNIS	5.75×10^{-3}	12.63	3100	1.3x
ACS	8.46×10^{-3}	28.47	2700	1.5x
HSCS	5.33×10^{-3}	19.01	3360	1.2x
Proposed	6.00×10^{-3}	8.88	170	24.1x

a learned prior, TabPFN produces reasonable approximations from about 100 samples, converges below 200 samples. This superior performance allows active learning to refine immediately and yield monotonic error reduction from the start.

Table 5 reports final performance consistent with the figure. Our zero-tuning framework achieves 8.88% MRE with 170 simulations, delivering a 24.1x reduction relative to the 4,100-sample MC baseline. HSCS requires 3,360 samples for 19.01% MRE, ACS 2,700 for 28.47%, MNIS 3,100 for 12.63%. Notably, our method matches OPT’s accuracy (8.88% MRE) while using over 17x fewer simulations.

Table 6: Ablation study demonstrating cross-corner knowledge transfer on 16×2 SRAM. Each target corner uses 50 samples from itself, plus 50 samples from an unseen corner.

Corner	Target Only	Additional Corners				MRE Reduction
		+1	+2	+3	+4	
TT	21.79	13.85	10.86	9.05	6.04	−72%
FF	0.00	0.00	0.00	0.00	0.00	—
SS	4.09	4.09	3.79	3.62	3.61	−12%
SF	100.00	100.00	71.43	57.14	42.86	−57%
FS	2.21	2.00	0.88	0.87	0.71	−68%

We collected 50 samples per corner (250 total for all 5 corners).

Importantly, many prior SOTA methods are developed and evaluated on idealized SRAM bitcells or toy circuits. Under non-ideal macro-level conditions, including input skew, large bitline loads, and noise from peripherals and neighbor cells, their gains diminish: in our realistic setup they deliver only 1.2–1.5x speedups with 12.63–28.47% MRE (Table 5). In contrast, our learned-prior approach remains accurate and data-efficient in the presence of second-order effects, confirming robustness and practical advantage in yield analysis.

4.3 Cross-Corner Knowledge Transfer

We measure whether training across PVT corners improves accuracy via knowledge transfer. Using the 16×2 SRAM, each target corner starts with 50 of its own samples, then incrementally adds 50 samples from additional unseen corners (from target-only to all five corners).

Table 6 shows that MRE decreases as the number of trained corners increases. For TT, MRE drops from 21.79% (target-only) to 6.04% (all corners, −72%); FS improves from 2.21% to 0.71% (−68%); SS from 4.09% to 3.61% (−12%). The challenging SF corner benefits most, falling from 100.00% to 42.86% (−57%). FF remains at 0.00% across settings, indicating it is already well-modeled without additional cross-corner data. These trends indicate that the proposed method leverages prior knowledge from correlated corners to improve accuracy and sample efficiency compared with per-corner training.

4.4 Scalable YMCA Validation

We evaluate the complete YMCA pipeline on four SRAM configurations (with 144 to 1152 variational parameters). For circuits exceeding 500 dimensions (16×2 and 32×2), we apply sparse feature selection, compressing to approximately 48 critical dimensions. All methods use identical simulation budgets: 1000-sample budgets for small circuits and 2500 for large; yield based on 50,000-sample MC is used as ground truth.

Table 4 demonstrates detailed yields and predictions across all PVT corners and SRAM configs. Our method maintains high accuracy everywhere: on low-dimensional circuits (4×2 , 8×2), it achieves best-in-class mean MRE of **0.11%** (4×2) and **0.22%** (8×2). On high-dimensional circuits where binary schemes collapse, our approach remains stable. On the 32×2 (1152D) benchmark, it reaches **1.10%** mean MRE while using fewer samples, keeping accuracy consistent across corner difficulties. PVT combinations strongly impact yield across sizes. For 8×2 , yield ranges from 99.0% (FF) down to 11.3% (SF) and collapses to 0% (SS); for 16×2 , SF is 0.14% while FS/FF are near 100%; for 4×2 , SS is 0% despite TT/FS at 100%; for 32×2 , SF is 34.9% versus 100% at FF/FS. Despite these swings, our method preserves accuracy across all PVTs and sizes, whereas binary baselines frequently fail at SF (e.g., 100% error on 16×2). This highlights the advantage of continuous performance modeling with learned priors in multi-corner settings.

5 CONCLUSION

We propose a novel yield analysis framework using learned priors to break the long-standing tuning barrier in yield analysis, achieving top performance with zero tuning and naturally enabling knowledge transfer to solve the YMCA challenges. Further improvements can be expected by fine-tuning TabPFN on SPICE simulation data from real circuits.

REFERENCES

- [1] Lara Dolecek, Masood Qazi, Devavrat Shah, and Anantha Chandrakasan. 2008. Breaking the simulation barrier: SRAM evaluation through norm minimization. In *2008 IEEE/ACM International Conference on Computer-Aided Design*. IEEE, 322–329.
- [2] Zhengqi Gao, Jun Tao, Dian Zhou, and Xuan Zeng. 2019. Efficient parametric yield estimation over multiple process corners via Bayesian inference based on Bernoulli distribution. *IEEE Transactions on Computer-Aided Design of Integrated Circuits and Systems* 39, 10 (2019), 3144–3148.
- [3] Fang Gong, Hao Yu, and Lei He. 2011. Stochastic analog circuit behavior modeling by point estimation method. In *Proceedings of the 2011 international symposium on Physical design*. 175–182.
- [4] Noah Hollmann, Samuel Müller, Lennart Purucker, Arjun Krishnakumar, Max Körfer, Shi Bin Hoo, Robin Tibor Schirmer, and Frank Hutter. 2025. Accurate predictions on small data with a tabular foundation model. *Nature* 637, 8045 (2025), 319–326.
- [5] Yanfang Liu, Guohao Dai, Yuanqing Cheng, Wang Kang, and Wei W Xing. 2023. OPT: Optimal Proposal Transfer for Efficient Yield Optimization for Analog and SRAM Circuits. In *2023 IEEE/ACM International Conference on Computer Aided Design (ICCAD)*. IEEE, 1–9.
- [6] Yanfang Liu and Wei W Xing. 2025. FUSIS: Fusing Surrogate Models and Importance Sampling for Efficient Yield Estimation. In *2025 Design, Automation & Test in Europe Conference (DATE)*. IEEE, 1–7.
- [7] Shan Shen, Xingyang Li, Zhuohua Liu, Yikai Wang, Yiheng Wu, Junhao Ma, Yuquan Sun, and Wei W Xing. 2025. OpenYield: An Open-Source SRAM Yield Analysis and Optimization Benchmark Suite. *arXiv preprint arXiv:2508.04106* (2025).
- [8] Jiahe Shi, Zhengqi Gao, Jun Tao, Yangfeng Su, Dian Zhou, and Xuan Zeng. 2020. Multi-corner Parametric Yield Estimation via Bayesian Inference on Bernoulli Distribution with Conjugate Prior. In *2020 IEEE International Symposium on Circuits and Systems (ISCAS)*. IEEE, 1–4.
- [9] Xiao Shi, Fengyuan Liu, Jun Yang, and Lei He. 2018. A fast and robust failure analysis of memory circuits using adaptive importance sampling method. In *Proceedings of the 55th Annual Design Automation Conference*. 1–6.
- [10] Xiao Shi, Hao Yan, Jinxin Wang, Xiaofen Xu, Fengyuan Liu, Longxing Shi, and Lei He. 2019. Adaptive clustering and sampling for high-dimensional and multi-failure-region sram yield analysis. In *Proceedings of the 2019 International Symposium on Physical Design*. 139–146.
- [11] Wei Wu, Srinivas Bodapati, and Lei He. 2016. Hyperspherical clustering and sampling for rare event analysis with multiple failure region coverage. In *Proceedings of the 2016 International Symposium on Physical Design*. 153–160.
- [12] Wei Xing, Yanfang Liu, Weijian Fan, and Lei He. 2024. Every Failure Is A Lesson: Utilizing All Failure Samples To Deliver Tuning-Free Efficient Yield Evaluation. In *Proceedings of the 61st ACM/IEEE Design Automation Conference*. 1–6.
- [13] Shuo Yin, Guohao Dai, and Wei W Xing. 2023. High-dimensional yield estimation using shrinkage deep features and maximization of integral entropy reduction. In *Proceedings of the 28th Asia and South Pacific Design Automation Conference*. 283–289.
- [14] Shuo Yin, Xiang Jin, Linxu Shi, Kang Wang, and Wei W Xing. 2022. Efficient bayesian yield analysis and optimization with active learning. In *Proceedings of the 59th ACM/IEEE Design Automation Conference*. 1195–1200.